Physicochem. Probl. Miner. Process., 5(55), 2019, 1323-1337

http://www.journalssystem.com/ppmp

Physicochemical Problems of Mineral Processing

ISSN 1643-1049

Received date April 15, 2019; reviewed; accepted date September 6, 2019

Effects of the fixed carbon and ash in blast furnace dust on its co-reduction with seaside titanomagnetite

Xiaoping Wang [1], Tianyang Hu [2], Chuanzhong Chen [2], Tichang Sun [3]

[1] School of Mining and Coal, Inner Mongolia University of Science and Technology, Baotou 014010, China

[2] State Environmental Protection Key Laboratory of Quality Control in Environmental Monitoring, China National Environmental Monitoring Centre, Beijing 100012, China

[3] School of Civil and Resource Engineering, University of Science and Technology Beijing, Beijing 100083, China

Corresponding author: 1362444061@qq.com (Tianyang Hu)

Abstract: Previous research has found that the fixed carbon in blast furnace dust (BFD) could be used as the reductant of co-reduction roasting of the iron oxides in seaside titanomagnetite and BFD to replace coals. This research studied the influence mechanism of the fixed carbon and ash in BFD on co-reduction. Results showed that both fixed carbon and ash in BFD promoted the reduction of iron, while ash had adverse effect on separation of titanium and iron. The main mechanism was as follows: The ash in BFD accelerated melting. In addition, the iron oxide in the ash of BFD could be reduced to metallic iron cores more easily in the initial stage, providing the site of inhomogeneous core and promoting the aggregation and growth of metallic iron. Furthermore, the fixed carbon mainly reacted with iron ore by solid-solid reaction, leading to a rapid reduction rate and a high utilization rate of fixed carbon.

Keywords: seaside titanomagnetite, blast furnace dust, co-reduction roasting, fixed carbon, ash

1. Introduction

Titanium is mainly recovered from rutile and ilmenite concentrates. However, high-grade rutile and ilmenite deposits are depleted, and their treating methods results in environmental pollution. Thus, the focus of attention is shifted to titanomagnetite (TTM) deposits, which is a source of titanium and iron. The Indonesian coastline contains numerous seaside TTM resources (Bryan et al., 2007; Cruz-Sánchez et al., 2004). Seaside TTM features high potential value, easy mining and low treatment cost, and thus can be used as raw materials for iron and steel making and titanium production (Dmitriev and Noskov 2017; Bryan et al., 2007).

Numerous studies were conducted to improve the utilization of TTM. Several new techniques, such as pyrometallurgical (Sun et al., 2017) and hydrometallurgical processes, acid leaching, and solvent extraction, have been studied (Kopkova et al., 2015; Lyberatos, 2007; Sun et al., 2013). However, these processes not only caused environmental pollution but also resulted in a serious waste of iron and titanium resources (Lyberatos 2007; Sun et al., 2013). The reduced iron powder (RIP), with high mass fraction and recovery was obtained through coal-based direct reduction followed by magnetic separation (Halli et al., 2017; Chen et al., 2011; Gao et al., 2016). Direct reduction is a practical and effective technique but depends on fixed carbon in coals (Gao et al., 2016). The consumption of coals as reductants increases process costs.

Blast furnace dust (BFD) is a kind of solid waste. BFD mainly contains iron and carbon as well as a small amount of silicon, aluminum, calcium, and magnesium (Zhang et al., 2017; Langov Aacute et al., 2010; Wu et al., 2016; Zhao et al., 2016). Approximately 10 million tons of BFD are produced annually from the blast furnace ironmaking industry in China (Langov Aacute et al., 2010). BFD used to be sent directly back into the blast furnace system as sintering raw material. Most domestic plants do not effectively use this material (Shen et al., 2013; Wu et al., 2016; Zhang et al., 2015; Zhao et al., 2016).

DOI: 10.5277/ppmp19060

Recently, replacing coal with BFD as reductant has been one of the hot research topics, as it contains carbon (Xing et al., 2018; Cao et al., 2018).

BFD can be used as the reductant to replace coal to reduce iron from BFD and seaside TTM synchronously during direct reduction, as it contains a certain amount of fixed carbon. Meanwhile, BFD contains iron oxides including magnetite and hematite. Thus, the direct reduction process of BFD and seaside TTM is called co-reduction roasting process. The co-reduction process is a new approach for highly effective utilization of BFD if its fixed carbon and iron oxides are used fully in co-reduction roasting. Hu et al. (Hu et al., 2017) utilized BFD as the reductant to study its co-reduction coasting with seaside TTM in Indonesia followed by magnetic separation. The results showed that the optimum conditions of roasting reduction included C/Fe molar ratio of 0.65, fluorite dose of 4 wt.%, and roasting temperature of 1300°C for 60 min. The reduced iron powder (RIP) and titania-rich slag were obtained through two-stage grinding and two-stage magnetic separation of the roasted ore. The former contained 94.23 wt.% of Fe and 0.58 wt.% of TiO_2 and showed total iron recovery of 87.62%. The latter contained Fe (19.72 wt.%) and TiO_2 (25.47 wt.%). Consequently, reduction was realized well using BFD, and the dosage of additives was reduced at the same time. It was found that BFD acts as a reductant during its co-reduction with seaside titanomagnetite, and the iron oxides in BFD were simultaneously reduced. Meanwhile BFD was favourable to separation of titanium and iron. In order to reveal the mechanism of co-reduction, the effects of the fixed carbon and ash contained in BFD in co-reduction roasting were investigated.

2. Materials and methods

2.1. Materials

2.1.1. Run-of-mine

The seaside TTM used in the present research was from Indonesia (here in after referred to as TTM). The valuable elements of TTM included Fe (53.51 wt.%), TiO_2 (11.26 wt.%). The mass fractions of CaO, MgO, SiO_2 and Al_2O_3 in TTM were 0.98 wt.%, 2.88 wt.%, 10.37 wt.%, and 5.73 wt.%, respectively. The occurrence state and microstructure of TTM were investigated by scanning electron microscopy, and energy dispersive spectroscopy (SEM-EDS) analysis, and the results are demonstrated in Fig. 1.

Fig. 1 indicates that the mineral grains are regularly shaped and uniform in TTM. In addition, most iron oxides have high degree of monomer dissociation with gangue, and a small amount of gangue minerals are embedded in the iron oxide grains. It was found, through EDS analysis, that Ti of TTM exists mainly in the form of isomorphism of iron hosting in the lattice of titanomagnetite. Furthermore, pure titanomagnetite grains are few, and most of them contain other elements such as Mg and Al. Many elements co-exist in the lattice of titanomagnetite, including Fe, Ti, Mg and Al, thus which are hardly separated through traditional methods.

2.1.2. Reductant

The reductants were the BFD from JiuQuan Steel and bitumite from Zhangjiakou. The particle size of bitumite was larger, with a size of 0.074 μm being occupied by 20.3 wt.%. In contrast, the mass fraction of a particle size of 0.074 μm in BFD was up to 31.4 wt.%. The industrial analysis results of BFD and bitumite were significantly different. The mass fraction of fixed carbon in BFD was only 26.31 wt.%, while that in bitumite was up to 50.07 wt.%. In addition, the mass fraction of ash in BFD was as high as 61.45 wt.%. However, in bitumite was only 11.76 wt.%, which was just one fifth of the former. The mass fractions of volatile in bitumite and BFD were 27.81 wt.% and 11.45 wt.%, respectively. The mass fraction of moisture was up to 10.36 wt.% in bitumite, and only 0.79 wt.% in BFD. BFD also contained a great deal of metallic element-iron, whose mass fraction was 27.69 wt.%. The mass fractions of CaO and MgO in BFD were 5.07 wt.% and 0.78 wt.%, respectively, and the mass fractions of SiO_2 and Al_2O_3 were 4.52 wt.% and 1.67 wt.%, respectively, while the mass fractions of CaO, MgO, SiO_2 and Al_2O_3 in bitumite were 1.83 wt.%, 0.25 wt.%, 1.1 wt.%, and 1.08 wt.%, respectively.

The mineral composition and microstructure of BFD and bitumite were analyzed and compared, as shown in Fig.s 2 and 3. Figure 2 indicates that the mineral composition of BFD is relatively complex. Both BFD and bitumite contain hematite, spinel and quartz. Additionally, BFD also comprises magnetite,

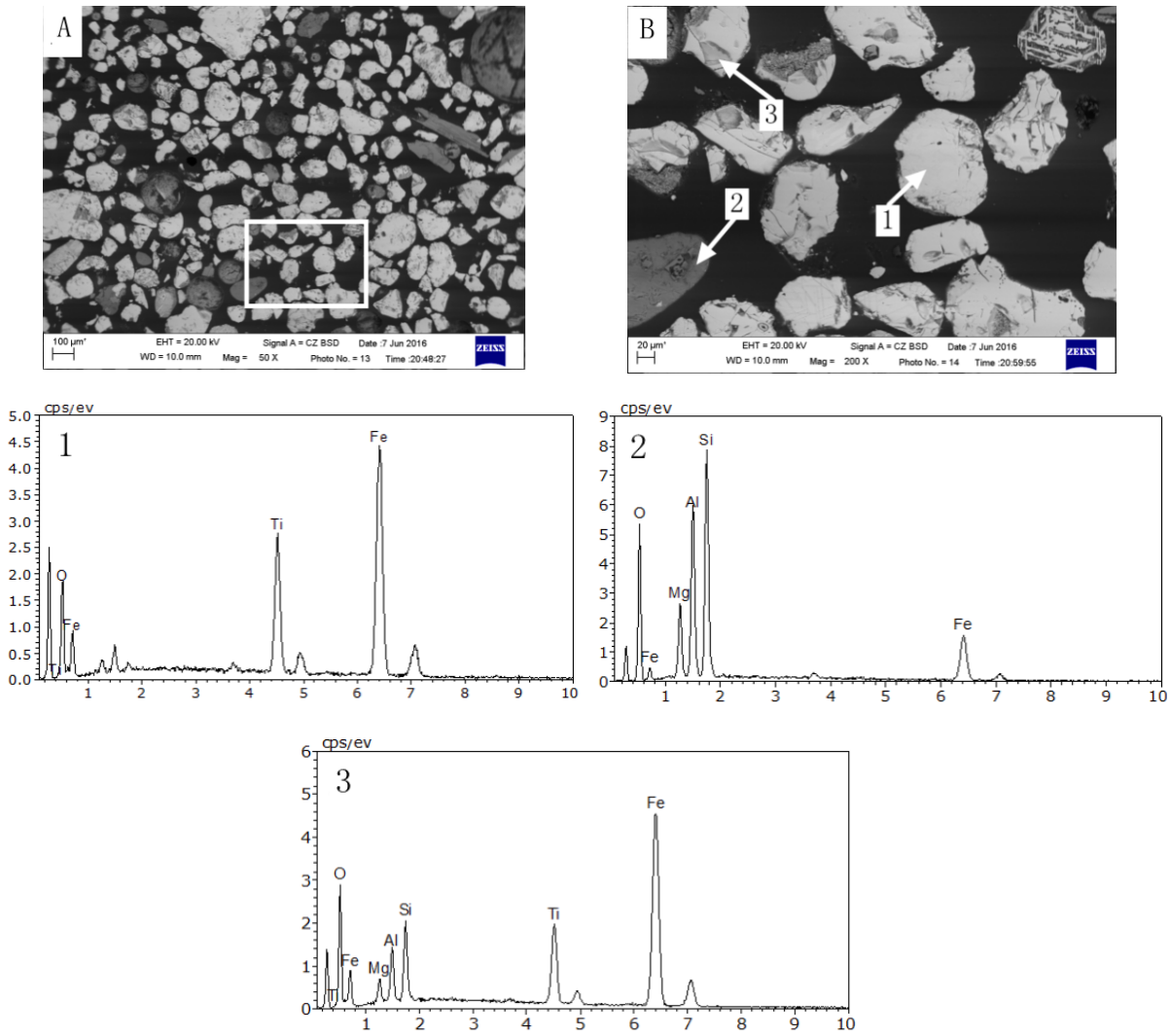

Fig. 1. SEM images of TTM: (A) in the scale of 100 µm; (B) in the scale of 20 µm; and EDS spectra for: (1,3) titanomagnetite ($Fe_{2.75}Ti_{0.25}O_4$) and (2) diopside $(Ca,Mg,Fe,Al)_2(Si,Al)_2O_6$)

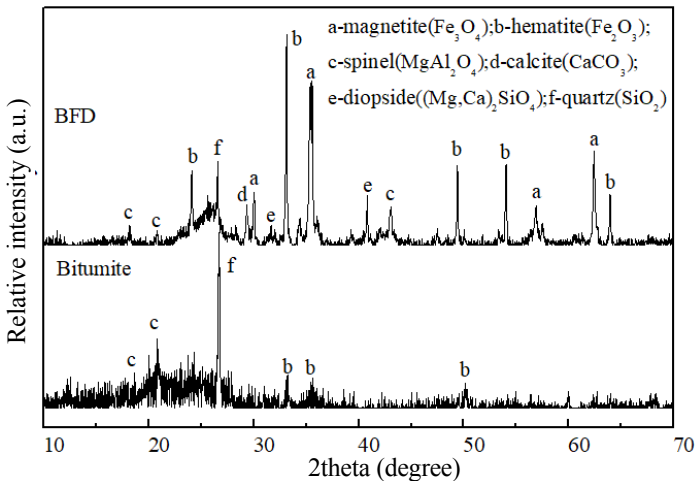

Fig. 2. XRD patterns of BFD and bitumite

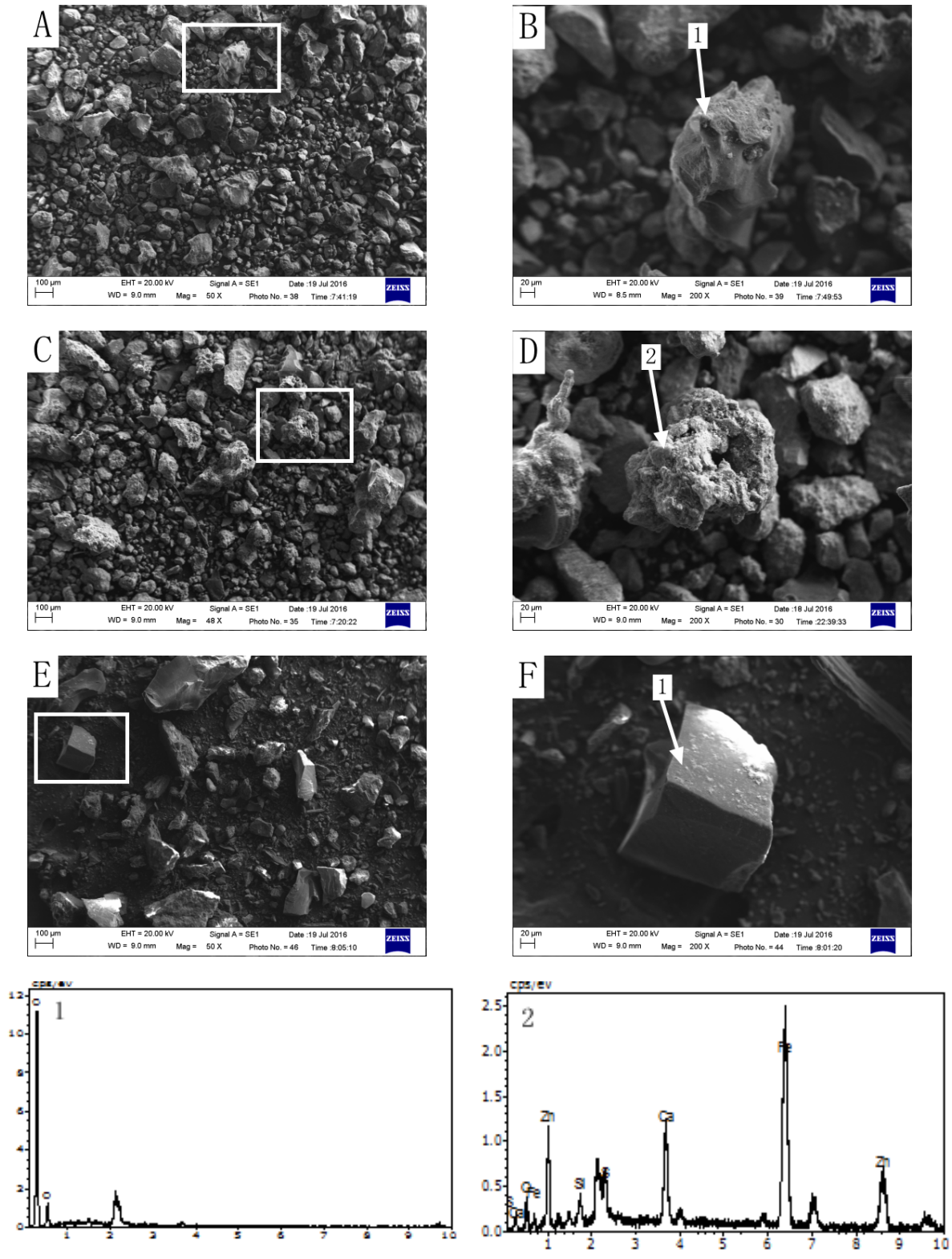

Fig. 3. SEM-EDS results of secondary electron of iron particles and carbon particles of BFD and bitumite: (A,B) carbon particles of BFD; (C,D) iron oxide particles of BFD and (E,F) bitumite

calcite, and olivine. According to images presented in Fig. 3, the particles of fixed carbon and iron oxide in BFD have rough surfaces and diverse shapes. A large number of iron oxide particles contain holes. Consequently, the surface areas of the fixed carbon and iron oxide in BFD are larger than those in bitumite. Given this, relatively speaking, the contact of the fixed carbon in BFD with iron oxide from

seaside TTM and BFD as well as the contact of the iron oxide in BFD with CO are more sufficient in the process of co-reduction roasting. EDS analysis was conducted on the iron oxide particles in BFD (Fig. 3(D), Point 2). The analysis results indicate that iron ore particles mainly contain Fe, Ca and O, as well as other impurities such as Si and Zn.

2.2. Research methods

2.2.1. Preparation of the carbon concentrate and iron concentrate from BFD

To investigate the influence mechanism of the fixed carbon and ash in BFD on co-reduction roasting followed by magnetic separation, the fixed carbon and ash in the BFD were separated through the flotation process. The flotation was carried out in a flotation machine, and the impeller rotation speed was set at 1800 rpm. With the flotation flowsheet of one roughing and one cleaning, the pulp concentration and the flotation temperature were 28 wt.% and 25°C, respectively. Kerosene and 2# oil were used as the collector and the frother, and their dosages were 1000 g/t and 60 g/t, respectively. The kerosene and 2# oil were added during roughing process, respectively. The foam product of the cleaner flotation was carbon concentrates (CFC), and the pulp in coarse flotation cell was iron concentrates (FT). Finally, the carbon concentrates and iron concentrates were filtered, dried at 80°C and weighed.

2.2.2. Reduction roasting and magnetic separation

According to previous studies (Gao et al., 2016; Hu et al., 2017), the C/O molar ratio was determined to be 0.65. The corresponding dosage of BFD was about 30 wt.%. The dosages of CFC and bitumite were 8.5 wt.% and 13.5 wt.% respectively, which were less than half the dosage of BFD. The dosages of BFD, bitumite, and CFC were the mass fraction relative to the seaside TTM. The sample seaside TTM was blended with BFD, bitumite, or CFC at the same C/O molar ratio (0.65), respectively. The mixture was placed in a crucible. Then 1 g of bitumite was covered on the surface of the mixtue and the crucible cover was utilized, cutting the mixture off from the air and keeping a reducing atmosphere. The diagram of the crucible is shown in Fig. 4. Then, the crucible was placed into the CD-1400X muffle furnace and roasted. The roasting temperature was determined to be 1250°C, and the roasting time was 60 min. The roasted ore was broken into particles with a size of smaller than 2 mm after natural cooling and then ground with a RK/BK roller four-cylinder intelligent rod mill. The ultimate fineness of the two-stage grinding was 43 μm, accounting for 69.02 wt.% of the total. The magnetic intensity of the two-stage weak magnetic separation was 151 kA·m^{-1}. After a magnetic separation using a CXG-99 magnetic tube, the magnetic product – RIP was obtained. The mass fraction of Fe, total iron recovery, and the mass fraction of TiO_2 in RIP were used as the indexes for the effects of the ash and fixed carbon in BFD on reduction as well as the separation of titanium and iron.

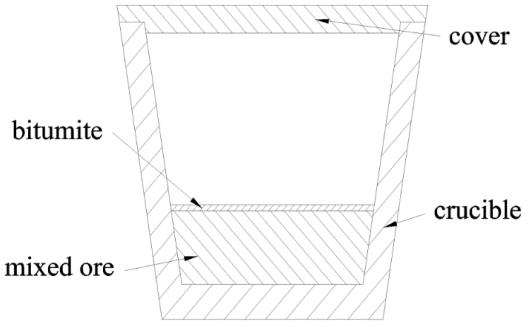

Fig. 4. The diagram of the crucible

The total iron recovery rate (Q) included the iron in TTM and the reductant, and was calculated by Eq (1). C/O mole ratio (n) was calculated by Eq (2). Here, m_1, m_2, m_3, and m_4 are the mass of seaside TTM, reductant, RIP, and covered bitumite, respectively; a_1, a_2, and β are mass fraction of iron in seaside TTM, reductant, and RIP, respectively; θ and δ are mass fractions of Fe_2O_3 and Fe_3O_4 in seaside TTM, respectively; ω and ε are mass fractions of Fe_2O_3 and Fe_3O_4 in reductant, respectively; λ and η are mass fractions of fixed carbon in reductant and covered bitumite, respectively.

$$Q = \frac{m_3 \times \beta}{m_1 \times \alpha_1 + m_2 \times \alpha_2} \times 100\% \quad (1)$$

$$n = \frac{(m_2 \times \lambda + m_4 \times \eta)/12}{(m_1 \times \theta + m_2 \times \omega)3/160 + (m_1 \times \delta + m_2 \times \varepsilon)/58} \quad (2)$$

2.2.3. XRD and SEM-EDS analyses

To perform mechanistic study, two samples were simultaneously roasted for each condition. One of the roasted ores was prepared into a powder sample and optical sheet to analyze the mineral composition and microstructure of the roasted ore. The XRD experiments were performed on a Japan Science Ultima IV diffractometer using Cu Ka radiation (k=1.5406 A), an operation voltage of 40 kV, and a current of 40 mA. The microstructure and particle size were determined using a scanning electron microscope (Zeiss EVO 18) equipped with energy dispersive spectroscopy (Quantax, Bruker, Germany).

2.2.4. Gas composition analysis

During gas determination, the crucible was put into the atmosphere furnace, heated from room temperature to 1250°C for 125 min and maintained at 1250°C for 60 min. In the meantime, nitrogen was injected into the atmosphere furnace at a flow rate of 4L/min. Concentrations of CO and CO_2 were detected with a MGA5/Vario plus infrared flue gas analyzer (MRU Messgeräte für Rauchgase und Umweltschutz GmbH, Neckarsulm, Germany).

3. Results and discussion

3.1. Properties of BFD carbon concentrate and iron concentrate

As presented in section 2.2.1, carbon concentrate (CFC) and iron concentrate (FT) were obtained from the BFD. The yields of CFC and FT were 40.83 wt.% and 21.84 wt.%, respectively. The mass fraction of fixed carbon in CFC was up to 77.81 wt.%, while the mass fraction of Fe was only 3.01 wt.%. In addition, the mass fractions of CaO, MgO, SiO_2 and Al_2O_3 in CFC were 2.16 wt.%, 0.97 wt.%, 10.53 wt.%, and 2.89 wt.%, respectively. The mass fraction of Fe in FT was as high as 47.03 wt.%, but the mass fraction of fixed carbon was only 0.46 wt.%.

X-ray diffraction analysis of CFC and FT were conducted, as shown in Fig. 5. The valuable minerals in FT are hematite and magnetite, and the gangue minerals mainly include olivine, spinel, quartz, and calcite. The valuable mineral in CFC is graphite, and the gangue minerals mainly include quartz, hematite, magnetite, and a small amount of spinel, diopside and calcite.

3.2. Effect of the fixed carbon and ash in BFD on co-reduction as well as titanium and iron separation

At the same C/O molar ratio of 0.65, the influence of the fixed carbon and ash in BFD on reduction as well as titanium and iron separation was studied. The reduction roasting effects using BFD and CFC as the reductants, respectively, were compared to analyze the effect of the ash, eliminating the influence factors of the fixed carbon. The comparison between the reduction roasting effects using CFC and bitumite as the reductants, respectively, was to study the influence of the fixed carbon in BFD, regardless of the effect of ash. The results are shown in Fig. 6.

Figure 6 indicates that the reduction as well as titanium and iron separation effects using BFD, CFC, and bitumite as the reductant, respectively, are significantly different at the same C/O molar ratio. Applying BFD as the reductant, the total iron recovery rate of the RIP obtained is up to 91.57%, and that obtained using CFC as the reductant is lower than 88%. The iron recovery rate of the RIP from bitumite is only 81.72%. The mass fractions of Fe in the RIP obtained from the three reductants are all above 90 wt.%, with a small difference of less than 2 wt.%. The mass fraction of Fe in the RIP obtained with using CFC as the reductant is the highest (up to 92.09 wt.%). The mass fractions of TiO_2 in the RIP obtained with using BFD and bitumite as the reductant are higher (above 1.3 wt.%) than that obtained using CFC as the reductant. The mass fraction of TiO_2 in the RIP obtained with using CFC as the reductant is only 0.86 wt.%.

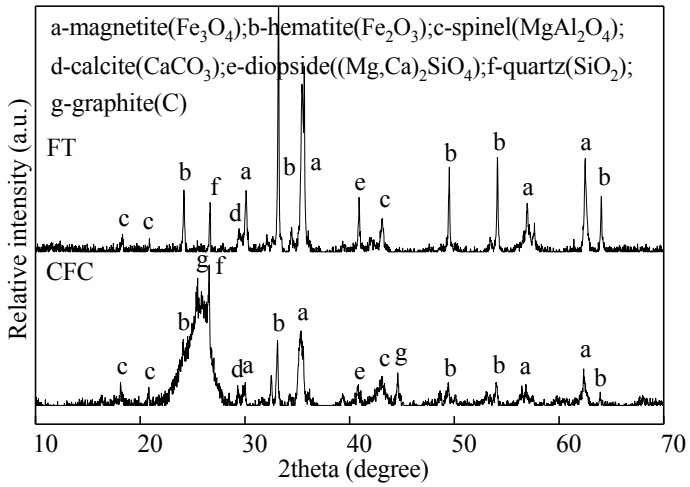

Fig. 5. X-ray diffraction patterns of CFC and FT

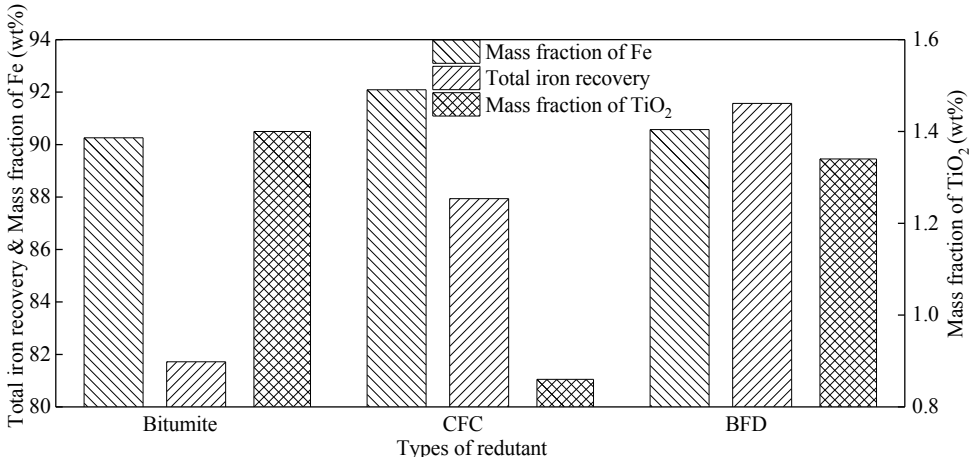

Fig. 6. Comparison of the effect of reduction as well as titanium and iron separation using BFD, CFC, and bitumite as the reductants, respectively

By comparing the RIPs obtained using bitumite and CFC as the reductants, respectively, the total iron recovery rate and the mass fraction of Fe in the latter was higher and the corresponding mass fraction of TiO_2 is lower. It indicates that the separation effect of titanium and iron is better when CFC is used as the reductant than that when bitumite is used as the reductant. Thus, the fixed carbon in BFD promotes the reduction of iron as well as the separation of titanium and iron.

Through a comparison between the RIPs obtained using BFD and CFC as the reductants, respectively, the total iron recovery of the former is higher and the corresponding mass fraction of TiO_2 is higher. It reveals that the reduction effect was better when BFD was used as the reductant, while the separation effect of titanium and iron was superior when CFC was used as the reductant. Consequently, the ash in BFD promotes the reduction of iron, but it is not conducive to separation of titanium and iron.

3.3. Mechanism of the fixed carbon and ash in BFD on co-reduction as well as titanium and iron separation

The results in Section 3.2 showed that the fixed carbon in BFD promotes reduction of iron as well as separation of titanium and iron; the ash in BFD promotes the reduction of iron, but it is not conducive to separate the titanium and iron. To reveal its mechanism, XRD and SEM-EDS analyses were conducted on the roasted ores obtained with using bitumite, CFC, and BFD as the reductants, respectively, as shown in Fig. 7 and 8.

As shown in Figs. 7 and 8, the mineral composition, microstructures and occurrence states of roasted ores obtained using the three kinds of reductants are different at the same C/O ratio.

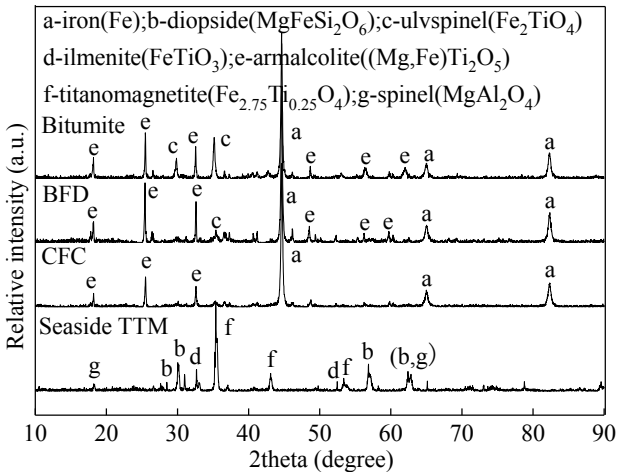

Fig. 7. XRD results contrast of the roasted ores using BFD, CFC, and bitumite as the reductants, respectively

In accordance to the mineral composition (Fig. 7), the titanium-bearing mineral contained in the roasted ores with CFC as the reductant is only armalcolite. However, those obtained using BFD and bitumite as the reductants, respectively, include armalcolite and ulvspinel. In addition, the diffraction peak of the ulvspinel in the roasted ores obtained using bitumite as the reductant is significantly higher than using BFD as the reductant. Ulvspinel contains a large number of Fe and TiO_2, which is not conducive to reduction as well as titanium and iron separation. These phenomena coincide with the phenomena of the best separation of titanium and iron when CFC is used as reductant (section 3.2), the worst separation of titanium and iron and the lowest recovery in RIP obtained when the bitumite is used as reductant (Fig. 6).

From the perspective of microstructure (Fig. 8), using BFD as the reductant, the melting phenomenon of the roasted ore is the most obvious, the metallic iron particles are the largest, and a large number of cyclic iron joined crystals are formed. Nonetheless, the cyclic iron joined crystals are wrapped with a large number of gangues and titanium-bearing minerals, hindering separation of titanium and iron. Thus, with BFD as the reductant, reduction effect is good, but the effects of titanium and iron separation is poor. Using CFC as the reductant, the metallic iron particles in the roasted ore obtained are large. Moreover, migration and aggregation happen to a small number of metallic iron grains. The iron joined crystals are formed, which gather at the edges of mineral particles. Only a small number of gangue and titanium-bearing minerals are wrapped in it. Consequently, reduction as well as separation effects of titanium and iron using CFC as the reductant are good. However, using bitumite as the reductant, a large number of titanium-bearing minerals are not reduced in the roasted ore obtained, and the size of metallic iron particles is the smallest, which are unevenly distributed in the gangue and titanium mineral slag phase. Therefore, with the bitumite as the reductant, the effects of reduction and separation of titanium and iron are both poor.

To sum up, the fixed carbon in BFD promotes the reduction of ulvspinel and the migration and aggregation of metallic iron particles. It is due to the rough surface, irregular shape, and the small particle size of the fixed carbon in BFD. Thus, the fixed carbons in BFD have a large surface area, increasing their contact area with iron oxides, so then, it is conductive to reduction.

The ash in BFD promotes melting as well as the migration and growth of metallic iron particles, leading to formation of iron joined crystals and being a source of disadvantage for separation of titanium and iron. The reason for that is as follows: the alkaline earth metal with high mass fraction in BFD improves the alkalinity of the mixture, which is the ratio of the mass fraction of the basic oxides to the acidic oxides. Studies have introduced that the suitable alkalinity range for direct reduction was determined to be 0.2~1.4 (Hu et al., 2014). Due to the low contents of MgO and Al_2O_3 (2.88 wt.% and 5.73 wt.% in TTM, 0.78 wt.% and 1.67 wt.% in BFD, 0.25 wt.% and 1.08 wt.% in bitumite, and 0.97 wt.% and 2.89 wt. % in CFC, respectively), it is mainly discussed as the binary alkalinity R= CaO/SiO_2. According to the experimental conditions in Section 3.2, the binary alkalinity is only 0.1 when the bitumite and CFC are used as the reductants, respectively. However, that is 0.2 when BFD is used as the reductant. An increase

of the binary alkalinity leads to reduction of the melting point and viscosity of the roasted ores, improving the conditions for growth and aggregation of metallic iron particles.

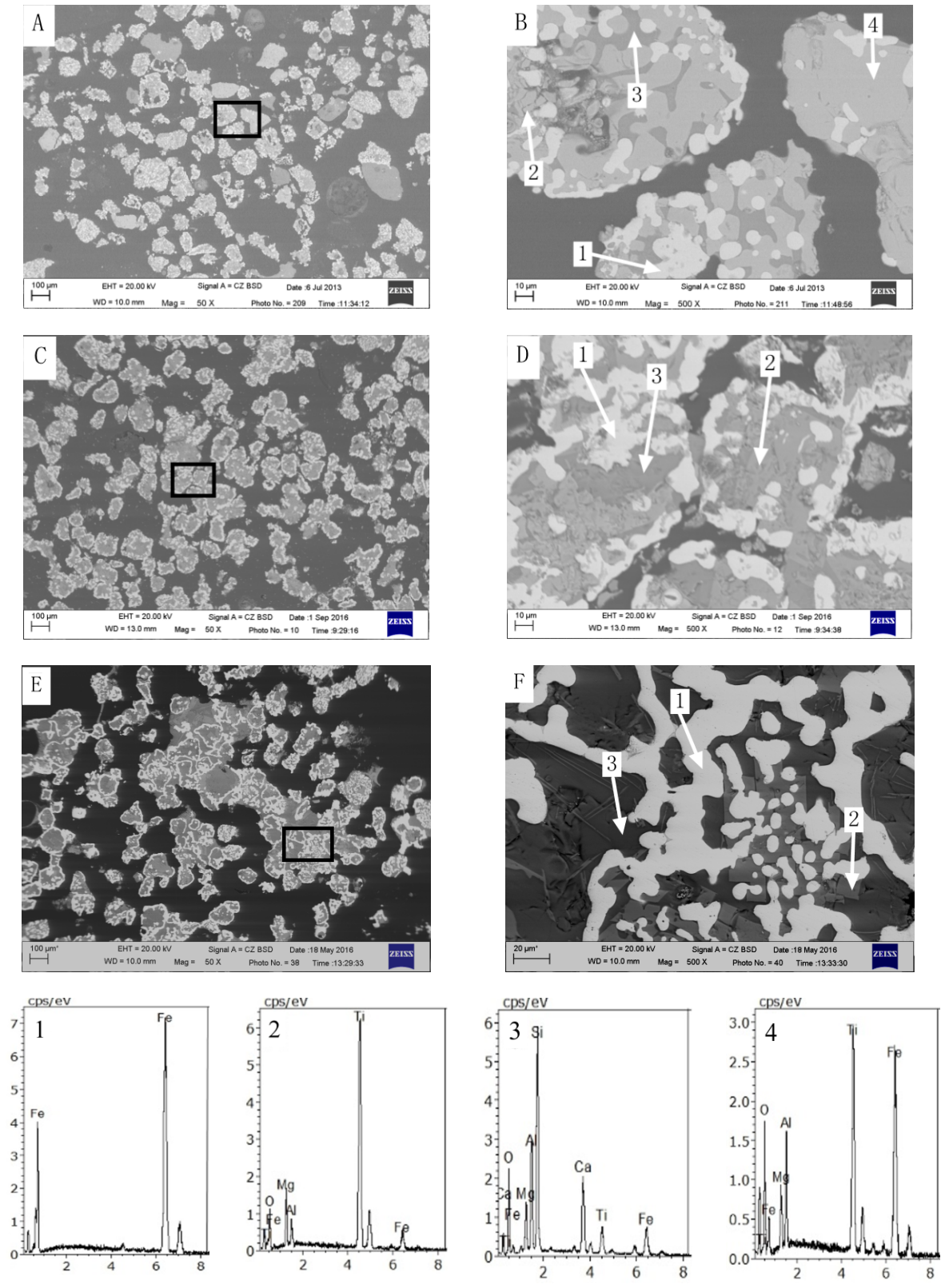

Fig. 8. SEM-EDS results contrast of the roasted ores obtained using BFD, CFC, and bitumite as the reductants, respectively: (A,B) bitumite; (C,D) CFC; (E,F) BFD, 1 – iron(Fe); 2 – armalcolite ($(MgFe)Ti_2O_5$); 3 – diopside $(Ca,Mg,Fe,Al)_2(Si,Al)_2O_6$; 4 – ulvspinel ($FeTi_2O_4$)

3.4. Effect mechanism of iron oxides in the ash of BFD on co-reduction

BFD also contains hematite and magnetite. In further research the influence mechanism of iron oxides in ash on co-reduction as well as titanium and iron separation effects, XRD and SEM-EDS analyses were conducted and compared with the roasted ores obtained from the reduction process of TTM and FT at different roasting times, respectively. CFC was used as the reductant. The roasting times were determined as 10, 20, 40, and 60 min, respectively. Other conditions were the same as the previous ones (Section 3.2). The results are shown in Figs. 9, 10 and 11.

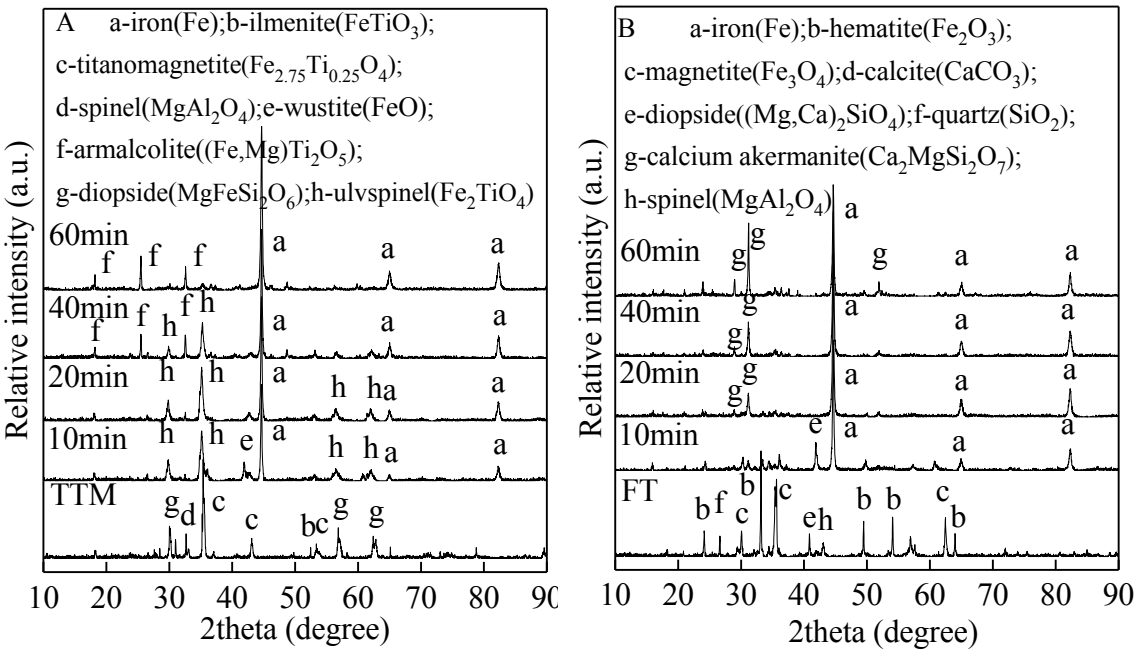

Fig. 9. Comparison of XRD patterns of the roasted ores of TTM and FT using CFC as the reductant, as a function of different roasting times: (A) TTM and (B) FT

As shown in Fig. 9A, the mineral compositions of roasted ore of TTM obtained as a function of different roasting times are different. At the 10th min, the main minerals in the roasted ore are ulvspinel, metallic iron, and wustite. At the 20th min, the diffraction peaks of wustite disappear, and at the 40th min, the diffraction peaks of ulvspinel weaken, and a small amount of armalcolite occurs. When the roasting time is prolonged to 60 min, the diffraction peaks of ulvspinel disappear, whereas the diffraction peaks of armalcolite obviously enhance. According to Fig. 9B, the mineral compositions of roasted ores of FT are relatively simple but significantly distinct as a function of different roasting times. At the 10th min, the main minerals in the roasted ore are metallic iron and diopside. At the 20th min, the diffraction peaks of diopside disappear and the diffraction peaks of calcium akermanite occur. When the roasting time is prolonged to 60 min from 20 min, the peak strength of metallic iron and calcium akermanite are enhanced continuously.

From Fig. 10, it can be seen that the microstructure and occurrence states of the roasted ore of seaside TTM with CFC as the reductant and at different roasting times are significantly different. The white particles are metallic iron (Point 1), light gray minerals are titanium-bearing minerals (Point 2 and Point 4), and dark gray minerals are gangue minerals (Point 3). At the 10th min, the particle size of metallic iron is small, and the boundary between metallic phase and slag phase is not clear. Clearly, at the 20th and 40th min, the metallic iron grains move outward from multiple growth centers, gradually growing from small particles into large ones and being non-uniformly distributed in slag phases of gangue and ulvspinel. At the 60th min, the metallic iron grains further diffuse, grow, gather around the mineral particles, and form iron joined crystals.

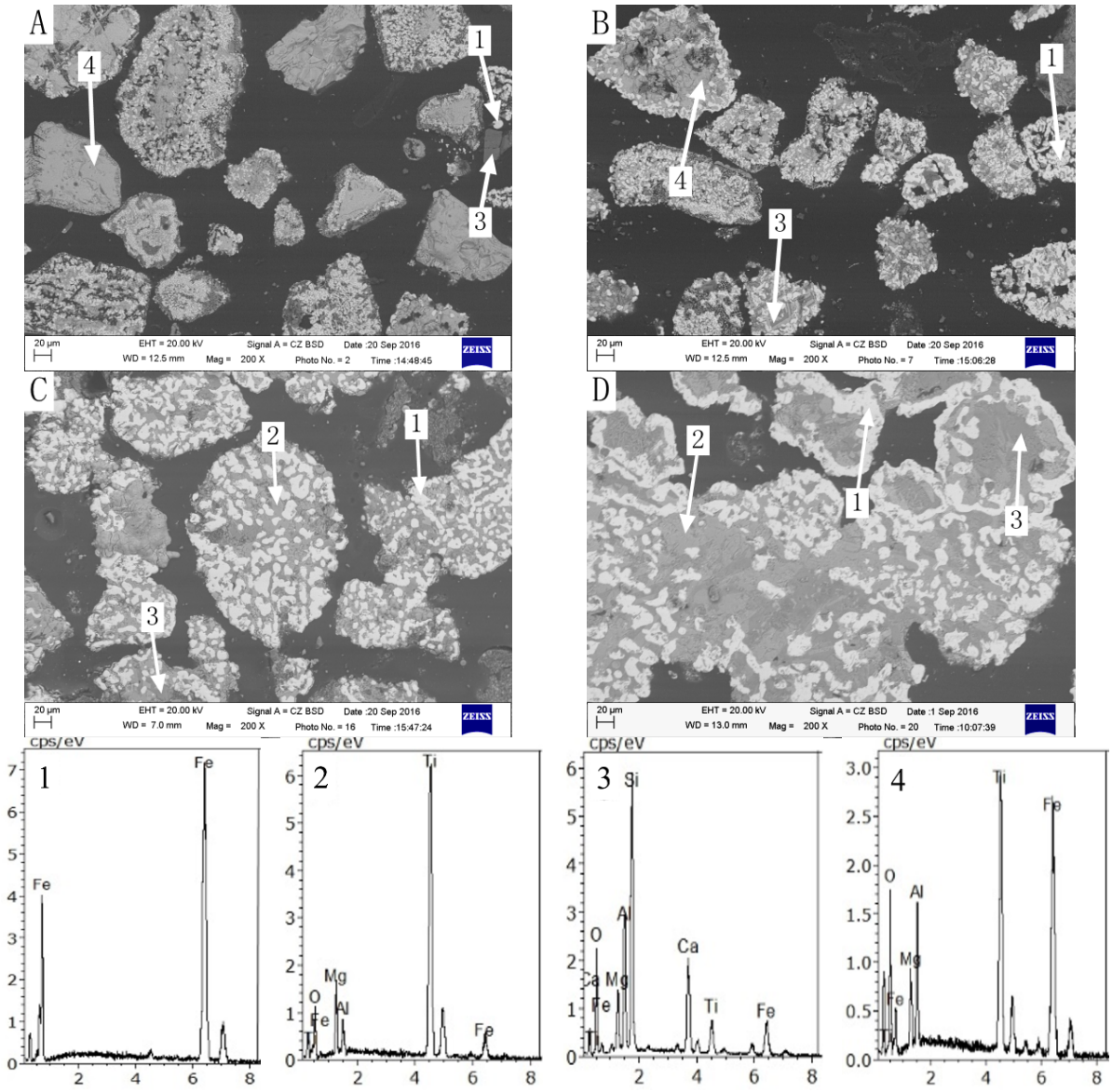

Fig. 10. SEM images of the roasted ore of TTM as a function of different roasting times: (A) 10 min; (B) 20 min; (C) 40 min; (D) 60 min, and EDS spectra for: 1 – iron (Fe); 2 – armalcolite ($(MgFe)Ti_2O_5$); 3 – diopside $(Ca,Mg,Fe,Al)_2(Si,Al)_2O_6$; 4 – ulvspinel ($FeTi_2O_4$).

Similarly, the microstructure and occurrence states of the roasted ore of FT are significantly different as a function of different roasting times (Fig. 11). However, unlike the roasted ore of seaside TTM, the slag phase of the roasted ore of FT melts at the 10th min. Though the particle size of metallic iron grain is also small, the boundary between the metal phase and the slag phase is clear. At the 20th min, the metallic iron grains obviously diffuse, gather, and form a small number of iron joined crystals. At the 40th min, the roasted ore melts obviously, and the metallic iron grains form contiguous iron joined crystals. At the 60th min, there is no obvious change.

According to results presented in Figs. 9, 10 and 11, the reduction of hematite and magnetite in FT separated from BFD through flotation is more easily than those in TTM. During reduction of FT, the iron crystal nucleus is formed early, which facilitate the forming of iron joined crystals. In addition, the melting point of slag phase is low, which conduce to melting. Some studies have shown that the formation of iron core not only provides the site for heterogeneous nuclear but also promotes the aggregation and growth of iron(Chuang et al., 2010; Hu et al., 2013). Thus, during co-reduction process of BFD and TTM, the iron oxides in BFD are reduced into iron core earlier.

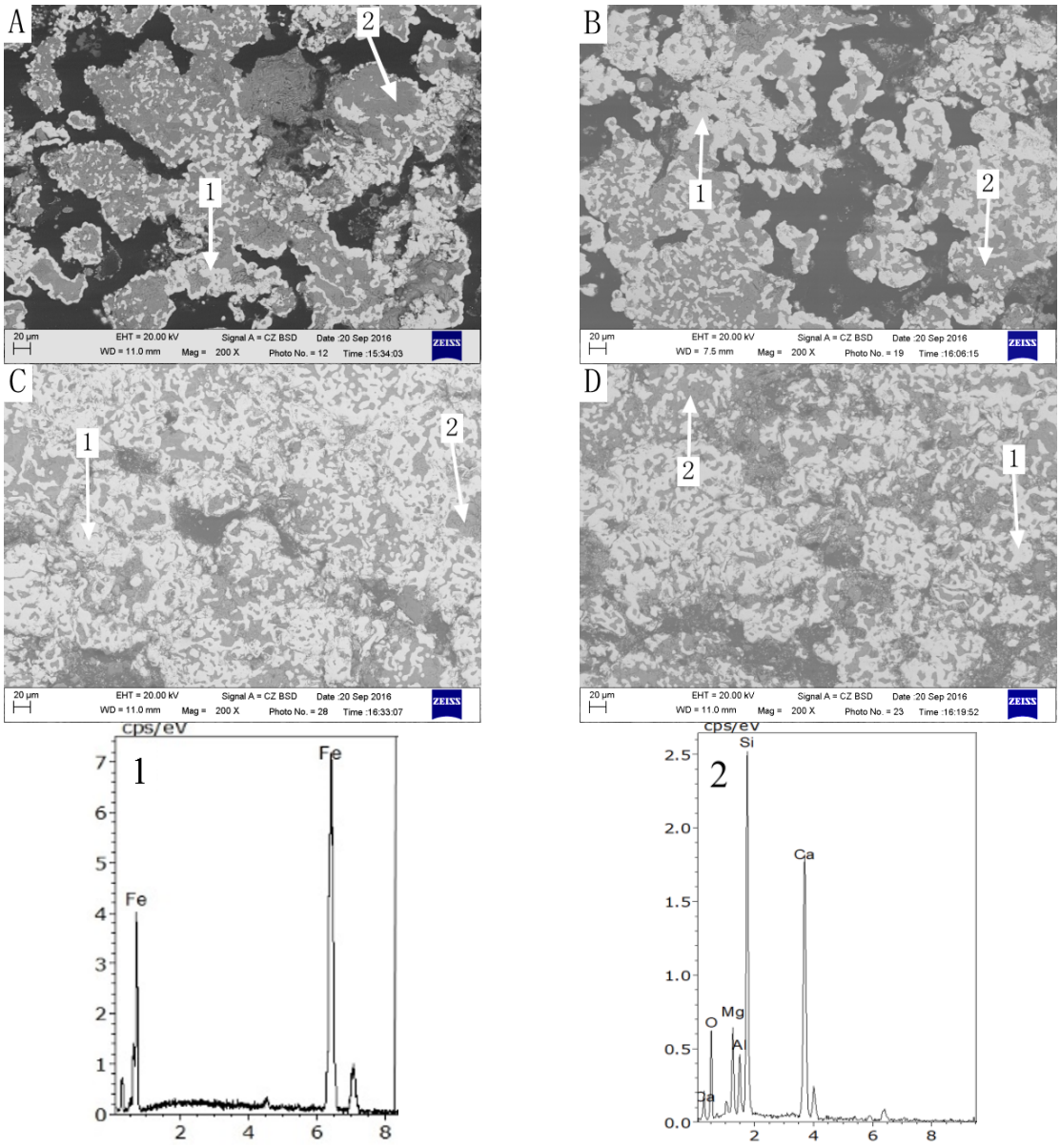

Fig. 11. SEM images of the roasted ore of FT as a function of different roasting times: (A) 10 min; (B) 20 min; (C) 40 min; (D) 60 min; and EDS spectra for: 1 – iron (Fe); 2 – calcium akermanite ($Ca_2MgSi_2O_7$)

3.5. Effect of the carbon presence in BFD on co-reduction

To further study the effect mechanism of the fixed carbon in BFD on its co-reduction roasting with TTM, the concentrations of CO and CO_2 in the gas generated, when using CFC and bitumite as the reductants, respectively, were analyzed and compared during co-reduction roasting. The roasting conditions were as follows: a C/O molar ratio of 0.65, a heating time of 125 min from room temperature to roasting temperature of 1250°C , and a duration of 60 min at 1250°C. The results are shown in Fig. 12.

As shown in Fig. 12, at the C/O molar ratio of 0.65, the concentrations of CO and CO_2 generated using CFC and bitumite as the reductant, respectively, are quite different. Due to the strong reactivity of bitumite, the initial temperature of CO generated is 900°C. However, that is 1033°C in the case of CFC. When bitumite was used as the reductant, the concentration of CO reaches its zenith at 1091°C, while when CFC was used as the reductant, it achieves its highest point at 1078°C. Remarkably, when using bitumite as the reductant, the CO concentration is still as high as 1.05 vol.% at the end of the roasting, indicating that the reduction reaction is not completed in the prescribed roasting time. This is also the reason for the low iron recovery rate of the RIP obtained using bitumite as the reductant.

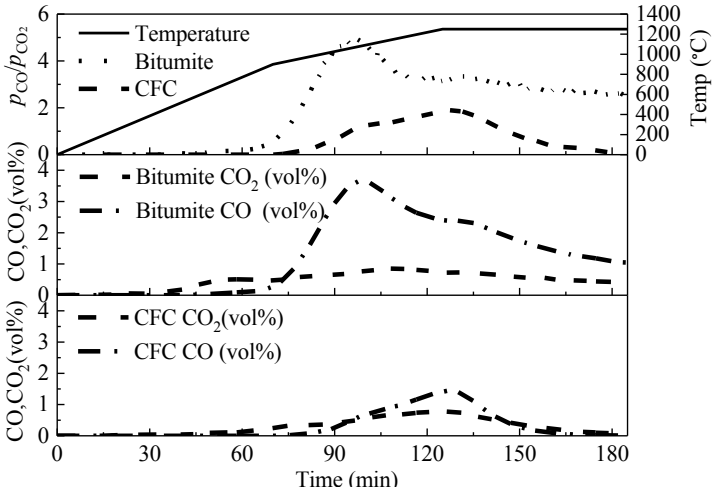

Fig. 12. Comparison of CO and CO_2 concentrations and p_{CO}/p_{CO2}, using CFC and bitumuite as the reductants, respectively

Using CFC as the reductant, the concentrations of CO and CO_2 are close to zero at the end of the roasting. Thus, although the initial reaction temperature is high and the gasification reaction rate is slow below 1250°C when CFC is used as the reductant, the reduction reaction is fast. By comparison, when BFD was used as the reductant, the CO concentration was low, and the CO_2 concentration was high. When the bitumite was used as the reductant, the largest concentrations of CO and CO_2 were 3.65 vol.% and 0.77 vo.l%, respectively. However, when CFC was used as the reductant, the CO and CO_2 concentrations were 1.45 vol.% and 0.78 vol.%, respectively. In general, the higher the concentration of CO, the stronger the reducing atmosphere, being favorable for the gas-solid reduction. By comparing the indexes of RIP, the reduction effect using CFC as the reductant is better than that in case of bitumite (Fig. 6). However, the CO concentration for the CFC is lower. This indirectly proves that solid-solid reaction is dominant when CFC is used as the reductant. By comparing P_{CO}/P_{CO2}, the relative concentration of CO_2 is higher when CFC is used as the reductant, which indicates a low gasification reaction rate. These phenomena show the carbon in CFC can not only restrain the gasification reaction, but also promote solid-solid reduction reaction.

To sum up, as compared with bitumite, the reaction activity of CFC is lower, and the gasification reaction of its carbon occurs at a higher temperature. Thus, solid-solid reduction reaction occurs at a longer time. In addition, with an increase of the roasting temperature, the liquid slag increases and Gibbs free energy promotes, which both enhance solid-solid reduction reactions which is conductive to accelerating the reaction rate, and thus the fixed carbon in CFC reacts fully and is used sufficiently.

To further compare the fixed carbon utilization rates using CFC and bitumite as the reductants, respectively, the ratio of reaction rate to gasification rate was studied. The reaction rate is expressed by V_R, which refers to the rate at which oxygen is removed from the iron oxide by fixed carbon. Gasification rate is expressed by V_G, which is the gasification speed of fixed carbon and CO_2 (Jung, 2014). Using bitumite and CFC as the reductants, respectively, their V_G/V_R results is calculated through their corresponding concentrations of CO and CO_2. The V_G/V_R results are compared as shown in Fig. 14. The reduction rate and gasification rate are calculated by Eqs. (3) and (4).

$$V_R(mol/\min) = \frac{vol_{CO}(\%/\min) + 2\times vol_{CO_2}(\%/\min)}{vol_{N_2}(\%/\min)} \times v_{N_2}(L/\min) \times \frac{1mol}{22.45L} \tag{3}$$

$$V_G(mol/\min) = \frac{vol_{CO}(\%/\min) + vol_{CO_2}(\%/\min)}{vol_{N_2}(\%/\min)} \times v_{N_2}(L/\min) \times \frac{1mol}{22.45L} \tag{4}$$

According to the above formulas, the ratio of the reaction rate to the gasification rate can reflect the utilization rate of fixed carbon. If the V_G/V_R curve is very close to that of V_G:V_R=1:2, it indicates that the final reduction reaction function can be approximately expressed as $Fe_xTi_yO_z+C=Fe_xTi_yO_{z-1}+CO_2$. It can be stated that 1 mol of C captures 2 mol of O from TiO_2-containing iron ores. Thus, the utilization rate

of fixed carbon is high. It can also be expressed that the lower the gasification rate and meanwhile the higher the reaction rate, the higher the utilization rate of fixed carbon is.

As shown in Fig. 13, it is obvious that the curve of CFC is closer to the straight line of V_G:V_R=1:2. In view of this, the utilization ratio of fixed carbon is higher when the CFC is used as the reductant than that when the bitumite is used as the reductant.

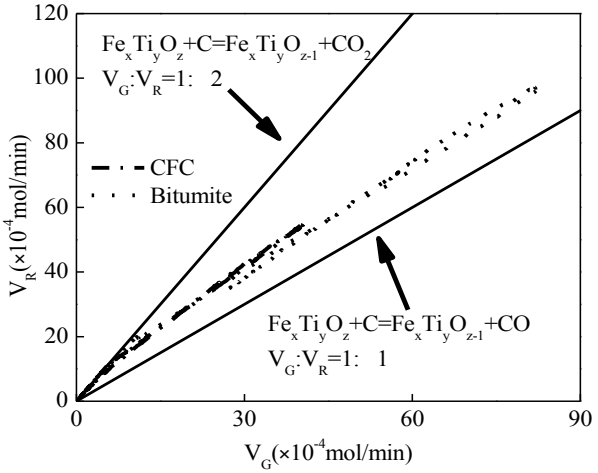

Fig. 13. Contrast of V_G/V_R results using bitumite and CFC as the reductants, respectively

4. Conclusions

At a same C/O molar ratio of 0.65, the indexes of the RIP obtained using BFD as the reductant were better than that in case of bitumite, and the effect of separation of titanium and iron using CFC as the reductant was the best. It indicates that the fixed carbon in BFD not only promoted reduction but also benefit separation of titanium and iron. Similarly, the ash in BFD promotes reduction, however, it was not conducive to separation of titanium and iron.

The mechanism was as follows. Due to the rough surface, irregular shape, and the small particle size, the fixed carbon in BFD had a lager surface area. This increased the contact area of the carbon with iron oxide particles. In addition, the fixed carbon mainly reacted with iron ore by solid-solid reaction, which was verified by comparing V_G/V_R results using bitumite or CFC as the reductant, respectively. It led to a rapid reduction rate and a high utilization rate of fixed carbon.

The alkaline earth metal with high mass fraction in the ash of BFD increased the alkalinity of roasted ores, reducing the melting point of roasted ores and thereby accelerating melting. In addition, the iron oxides including hematite and magnetite in the ash of BFD was reduced easily to form iron nucleus at the initial stage of reduction, providing the sites for heterogeneous nucleus and promoting the aggregation and growth of metallic iron. Thus, a large number of cyclic iron joined crystals were formed, and gangues and titanium-bearing minerals were wrapped in them, thereby being not conductive to separation of titanium and iron.

Acknowledgments

The authors wish to thank the National Natural Science Foundation of China (NSFC) for funding this research (No. 51874017).

References

BRYAN, K.R., ROBINSON, A., BRIGGS, R.M., 2007. *Spatial and temporal variability of titanomagnetite placer deposits on a predominantly black sand beach.* Mar. Geol. 236, 45-59.

CAO, Y.Y., DUAN, D.P., ZHOU, E., SUN, T.C., 2018. *The function of blast furnace dust as reductant on simultaneous reduction of high-phosphorus oolitic hematite*. Ironmak. Steelmak. 1-11.

CHEN, D.S., SONG, B., WANG, L.N., QI, T., WANG, Y., WANG, W.J., 2011. *Solid state reduction of Panzhihua titanomagnetite concentrates with pulverized coal*. Miner. Eng. 24, 864-869.

CHUANG, H., HWANG, W., LIU, S., 2010. *Effects of graphite, SiO_2, and Fe_2O_3 on the crushing strength of direct reduced*

iron from the carbothermic reduction of residual materials. Mater. Trans. 51, 557-563.

CRUZ-SÁNCHEZ, E., ÁLVAREZ-CASTRO, J.F., RAMíREZ-PICADO, J.A., MATUTES-AQUINO, J.A., 2004. *Study of titanomagnetite sands from Costa Rica*. J. Alloy. Compd. 369, 265-268.

DMITRIEV, A.N., NOSKOV, V.Y., 2017. *Physicochemical and thermophysical bases of titanomagnetite ore treatment*. Metallurg. 61, 382-386.

GAO, E., SUN, T., LIU, Z., GENG, C., XU, C., 2016. *Effect of sodium sulfate on direct reduction of beach titanomagnetite for separation of iron and titanium*. J. Iron Steel Res. Int. 23, 428-433.

HALLI, P., TASKINEN, P., ERIÇ, R.H., 2017. *Mechanisms and kinetics of solid state reduction of titano magnetite ore with methane*. J. Sustain. Metall. 3, 191-206.

HU, T., LV, X.W., BAI, C.G., QIU, G. B., 2014. *Isothermal reduction of titanomagnetite concentrates containing coal*. Int. J. Min. Met. Mater. 21, 131-137.

HU, T., LV, X., BAI, C., LUN, Z., QIU, G., 2013. *Carbothermic reduction of titanomagnetite concentrates with ferrosilicon addition*. ISIJ Int. 53, 557-563.

HU, T., SUN, T., KOU, J., CHAO, G., WANG, X., CHAO, CH., 2017. *Recovering titanium and iron by co-reduction roasting of seaside titanomagnetite and blast furnace dust*. Int. J. Miner. Process. 165, 28-33.

JUNG, S., 2014. *Thermogravimetry and reaction gas analysis of the carbothermic reduction of titanomagnetite ores with char*. ISIJ Int. 54, 781-790.

KOPKOVA, E.K., SHCHELOKOVA, E.A., GROMOV, P.B., 2015. *Processing of titanomagnetite concentrate with a hydrochloric extract of n-octanol*. Hydrometallurgy 156, 21-27.

LANGOVA, S., MATÝSEK, D., 2010. *Zinc recovery from steel-making wastes by acid pressure leaching and hematite precipitation*. Hydrometallurgy. 101, 171-173.

LYBERATOS, A., 2007. *Temperature dependence of the magnetization of titanomagnetites*. J. Magn. Magn. Mater. 311, 560-564.

SHEN, L., QIAO, Y., YONG, G., TAN, J., 2013. *Preparation and formation mechanism of nano-iron oxide black pigment from blast furnace flue dust*. Ceram. Int. 39, 737-744.

SUN, H., ADETORO, A.A., PAN, F., WANG, Z., ZHU, Q., 2017. *Effects of high-temperature preoxidation on the titanomagnetite ore structure and reduction behaviors in fluidized bed*. Metall. Mater. Trans. B. 48, 1-10.

SUN, H., WANG, J., HAN, Y., SHE, X., XUE, Q., 2013. *Reduction mechanism of titanomagnetite concentrate by hydrogen*. Int. J. Miner. Process. 125, 122-128.

WU, Z.J., WANG, L.C., GAO, Z.F., LIU, W.M., WU, X.R., 2016. *Recycling blast furnace dust into metals (Al, Zn and Ti)-doped hematite with enhanced photocatalytic activity*. J. Environ. Chem. Eng. 4, 341-345.

XING, X.D., CHEN, Y.F., LIU, Y.R., 2018. *Study of the reduction mechanism of ironsands with addition of blast furnace bag dust*. Metall. Res. Technol. 115, 214-222.

ZHANG, D., ZHANG, X., YANG, T., RAO, S., HU, W., LIU, W., CHEN, L., 2017. *Selective leaching of zinc from blast furnace dust with mono-ligand and mixed-ligand complex leaching systems*. Hydrometallurgy 169, 219-228.

ZHANG, Y., LI, S., WANG, X., LI, X., 2015. *Coagulation performance and mechanism of polyaluminum ferric chloride (PAFC) coagulant synthesized using blast furnace dust*. Sep. Purif. Technol. 154, 345-350.

ZHAO, D., ZHANG, J., WANG, G., CONEJO, A.N., XU, R., WANG, H., ZHONG, J., 2016. *Structure characteristics and combustibility of carbonaceous materials from blast furnace flue dust*. Appl. Therm. Eng. 108, 1168-1177.